Korean J. Chem. Eng., **27**(2), 416-421 (2010)
DOI: 10.1007/s11814-010-0110-1

Scaling behavior of a wormlike polyelectrolyte chain by mesoscopic Brownian dynamics simulations

Myung-Suk Chun†

Complex Fluids Research Laboratory, Korea Institute of Science and Technology (KIST),
Seongbuk-gu, Seoul 136-791, Korea
(*Received 12 October 2009 • accepted 1 December 2009*)

Abstract−The scaling prediction of semiflexible wormlike chain was examined by applying Brownian dynamics simulation, which goes beyond other simulations as they do not consider both the hydrodynamic interaction between pairs of beads and long-range screening effect. The rheological behavior of the intrinsic viscosity was properly implemented by combining with optimized model parameters for the polyelectrolyte xanthan, and the validity of the simulation was previously confirmed. Scaling plots present that the structure and diffusion of polyelectrolyte chains depend sensitively on the Debye screening effect. In the scaling of end-to-end distance R_E, radius of gyration R_G, and translational diffusivity D_T with respect to the number of beads N_b, the Flory-Edwards exponent ν was estimated as up to 1.0, which should be a really higher level compared to the case of the flexible neutral chains with self-avoiding walk in good solvent. Unlike the case of spherically averaged structure factor, scaling plots in that parallel to the first principal axis of gyration could not clearly be identified with a well defined exponent. With increasing screening effect, pronounced oscillations observed in the case of lower screening tend to smear out.

Key words: Polyelectrolyte, Scaling Theory, Chain Conformation, Coarse-graining, Brownian Dynamics Simulation

INTRODUCTION

Polyelectrolytes represent an interesting and broad class of soft matter that should be considered as an additional complication arising from the Debye screening of long-range electrostatic interaction by ions [1-4]. These characteristics prevent a direct application of many reliable theories developed for neutral polymers, although polyelectrolytes have stimulated interest from a fundamental as well as from a technological point of view. It is usually necessary to consider more system-specific aspects such as the surface charge, solution rheology, and the condensation of counterions and salt ions. A precise understanding of charged soft matter has received great attention in life science and molecular biology because proteins, and other biopolymers such as DNA or polysaccharide, are polyelectrolytes.

Long ago, numerous theoretical and computational studies presented the scaling behavior of neutral polymer chains with a self-avoiding walk (SAW), analyzing the structural and the rheological properties based on the bulk scaling [5-8]. We abbreviate the review of the scaling predictions for linear polymers by considering a polymer of N monomers with persistence length l_P and molecular weight (i.e., Mw ~ N). In bulk, the polymer attains a coiled configuration with a radius of gyration $R_G \sim l_P N^{\nu}$). Here, the universal exponent ν is the Flory-Edwards exponent (cf., ν=3/5 for a good solvent, 1/2 for an ideal theta solvent, and 1/3 for a poor solvent) [9]. Scaling of diffusivity with Mw isolates the effect of a hydrodynamic interaction (HI). The scaling behavior in confined spaces has also been investigated [10-12]. The structure of confined polyelectrolytes underlying a finite rigidity due to intrachain repulsion has been examined under two-dimensional (2D) confinement [10]. A more advanced theory and lattice Monte Carlo simulations showed that a crossover from an unbounded to a confined space exhibited a non-monotonic size variation with a minimum when the narrow slit width was comparable to the end-to-end distance of the chain in the bulk [11].

Simulation studies using the Brownian dynamics (BD) method with HI have improved the understanding of how a single polyelectrolyte chain behaves. In modeling the properties of the polyelectrolyte solution, the solvent is treated as a continuum, while the molecule is usually represented by a coarse-grained model such as a bead-spring chain [13-15]. The biological macromolecules are currently well-used as the model polyelectrolyte. By the way, previous studies were almost confined to an analysis of the equilibrium conformation and the diffusion of a single DNA molecule with a contour length of above 4 μm. This is due to the advancement of micro/nanofluidic devices for DNA manipulations. Jendrejack et al. [16,17] found the effect of a length scale associated with polymer-wall interactions because the scalings obtained did not match the theoretical predictions in square channels. Chen et al. [18] examined the diffusion of double stranded DNA molecules in slitlike channels with variations in channel height and molecular weight.

Recently, the author's group has examined the conformation and dynamic properties of a single chain of xanthan polyelectrolytes by employing simulations as well as experimental observations. Jeon and Chun [19] developed coarse-grained BD simulations of polysaccharide xanthan polyelectrolytes in bulk solution as well as under con-

†To whom correspondence should be addressed.
E-mail: mschun@kist.re.kr
‡This paper is dedicated to Professor Jae Chun Hyun for celebrating his retirement from Department of Chemical and Biological Engineering of Korea University.

finement, taking into account the HIs between pairs of beads. Xanthan is generally accepted as semiflexible due to the double stranded structure with intrinsic persistence length of at least 100 nm [20, 21]. It has up to two ionizable carboxyl groups per repeat unit, and the side chains give a semi-rigid character to the main chain. They have quantified the chain conformation and translational diffusion, from which the structural transition of a chain from unbounded to confined states has been elucidated with emphasizing the influence of chain intrinsic rigidity. By single molecule tracking with epi-fluorescence microscopy, experimental verifications were performed by Chun et al. [22]. It was found that their simulation on the conformational changes of xanthan chain had a reasonable trend to agree with experiments. The experimental diffusivity revealed lower values than the simulation results perhaps due to unavoidable restrictions; however, considering the consistency with literature values could confirm the validity of their BD simulations.

In this research, scaling predictions for the chain conformation and diffusion of wormlike polyelectrolyte are investigated with respect to a chain length of xanthan. The influence of ionic strength of surrounding medium is highlighted, since the structure of polyelectrolytes in solvent is governed by screening effect pertaining to the long-range interaction and correlated displacement. Brownian motion of the molecules is basically described within the framework of Kirkwood's theory [6,23]. Hence, it is possible that our BD simulations estimate the translational diffusion coefficient of chain with an HI between beads and excluded volume. Additional result devoted to the estimation of structure factor is addressed, which can serve as a basis for further understanding the behavior of soft matter.

GROBAL PROPERTIES OF POLYELECTROLYTE CHAIN

As shown in Fig, 1, structural properties of the xanthan chain can be the root-mean-square end-to-end distance R_E and radius of gyration R_G [6] for each position of n-th bead $\mathbf{r}_n$ with N_b beads, given by

$$R_E = \left\langle (\mathbf{r}_{N_b} - \mathbf{r}_1)^2 \right\rangle^{1/2} = \left\langle \left(\sum_{n=1}^{N_b} \mathbf{r}_n \right)^2 \right\rangle^{1/2}, \quad (1)$$

$$R_G^2 = \frac{1}{N_b} \sum_{n=1}^{N_b} \left\langle |\mathbf{r}_n - \mathbf{R}_{CM}|^2 \right\rangle. \quad (2)$$

Here, the position of the center-of-mass is

$$\mathbf{R}_{CM} = \left(\sum_{n=1}^{N_b} \mathbf{r}_n \right) \Big/ N_b. \quad (3)$$

The theoretical scaling for these properties is $\langle R_E^2 \rangle \propto \langle R_G^2 \rangle \propto N_b^{2\nu}$, where the value of ν has 0.588 for the SAW in good solvent from renormalization group theory methods [7]. Further, the contour length R_C is given by

$$R_C = (N_b - 1)b = \sum_{n=1}^{N_b-1} b_n = \sum_{n=1}^{N_b-1} |\mathbf{r}_{n+1} - \mathbf{r}_n| \quad (4)$$

where b and b_n mean the average bond and n-th bond length, respectively. Note that the contour length R_C can vary with medium ionic strength due to the variable screening of bead-bead electrostatic interactions.

As described in detail in the previous studies [19,22], the persistence length l_P can be determined from the average contour distance between beads separated by n bonds. The correlation length of bond vectors separated by n bonds provides a useful measure of the relative strength of short- and long-range bond vector correlations. It becomes independent of n only when the bond vector correlation decays exponentially on the entire length scale [24].

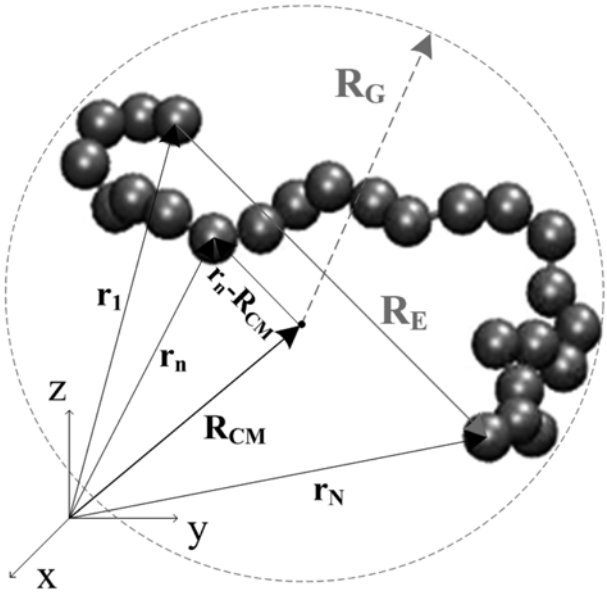

Fig. 1. Schematic of conformation parameters in coarse-grained polyelectrolyte chain.

The self-diffusion coefficient provides important information on the chain structure as well as dynamics. From the Kirkwood formula [23], the short-time diffusion coefficient is obtained by averaging over the trace

$$D_T = \frac{1}{3N_b^2} \sum_{i,j} \mathrm{Tr} \langle \mathbf{D}_{ij} \rangle. \quad (5)$$

In the long-time limit within Cartesian coordinates system, the diffusive motion of the Brownian particle is parameterized by its translational self-diffusion coefficient through the Einstein-Smoluchowsky relation [6,25],

$$D_{T,\beta} = \lim_{\delta t \to \infty} \frac{1}{2\delta t} \left\langle [R_{CM,\beta}(t) - R_{CM,\beta}(t - \delta t)]^2 \right\rangle \text{ for } \beta = x, y, z. \quad (6)$$

Here, δt is the lag time and the average $\langle \cdots \rangle$ is the mean-square displacement (MSD) carried out over the entire trajectory. To better compare the experimental results with simulations, 2D diffusion coefficients $D_T^{2D} = (\sum_{\beta=x,y} D_{T,\beta})/2$ can be considered in bulk. The full 3D diffusion coefficient is found to be different from the 2D one with x and y components by less than 2%, if the limit $\delta t \to \infty$ on the right-hand side of Eq. (6) is replaced by δt=0.2 msec.

BROWNIAN DYNAMICS SIMULATION OF XANTHAN POLYELECTROLYTE

1. Coarse-Graining Procedure

Here, a brief review is provided regarding the coarse-grained mesoscopic model of polyelectrolytes with polysaccharide xanthan em-

ployed in the prior works [19,21], in which the xanthan was modeled as a bead-spring chain composed of uniformly charged monomers. The generalized Langevin equation provides the reference for the generation of molecular trajectories in a dielectric continuum of the solvent medium.

The dynamics of xanthan chain is described by the following BD equation of motion that accounts for the bead-bead fluctuating HI through the Ermak and McCammon algorithm [26],

$$\mathbf{r}_i^{n+1}=\mathbf{r}_i^n+\Delta t\left[\sum_j\frac{\mathbf{D}_{ij}^n\cdot\mathbf{F}_j^n}{k_BT}+\sum_j\nabla_j\cdot\mathbf{D}_{ij}^n+\mathbf{G}\cdot\mathbf{r}_i^n\right]+\mathbf{R}_i^n \tag{7}$$

where subscripts i and j represent each bead. $\mathbf{F}_j^n=-\nabla E^{Total}(t_n)$ is the total force on bead at time step n, $\mathbf{R}_i^n$ is the random displacement due to the solvent, Δt is the time step size, and k_BT is the Boltzmann thermal energy. The velocity field created from the motion of a segment of the xanthan molecule is taken to be due to a chain of point forces acting on the fluid. The bead-bead HI is adequately represented by a chain of point forces (Stokeslets). Instead of the Oseen-Burgers tensor (i.e., free-space Green's function), the Rotne-Prager diffusion tensor $\mathbf{D}_{ij}^n$ is employed to describe the HI between beads [27], representing positive-definite for all chain configurations. With formulating 3×3 block components of the $3N_b\times3N_b$ matrix, it can be expressed as

$$\mathbf{D}_{ij}=k_BT\left(\frac{1}{6\pi\eta a}\mathbf{I}\delta_{ij}+\Omega_{ij}\right) \tag{8}$$

where η is the solvent viscosity, $\mathbf{I}$ is the unit tensor, and Ω_{ij} is the HI tensor. The HI tensor relates the velocity perturbation at point $\mathbf{r}_i$ to a point force at $\mathbf{r}_j$:

$$\Omega_{ij}=\frac{1}{8\pi\eta r_{ij}}\left[\left(1+\frac{2a^2}{3r_{ij}^2}\right)\mathbf{I}+\left(1-\frac{2a^2}{r_{ij}^2}\right)\frac{\mathbf{r}_{ij}\mathbf{r}_{ij}}{r_{ij}^2}\right]\ (i\neq j, r_{ij}>2a), \tag{9a}$$

$$\Omega_{ij}=\frac{1}{8\pi\eta r_{ij}}\left[\frac{r_{ij}}{2a}\left(\frac{8}{3}-\frac{3r_{ij}}{4a}\right)\mathbf{I}+\frac{r_{ij}^2}{8a^2}\frac{\mathbf{r}_{ij}\mathbf{r}_{ij}}{r_{ij}^2}\right]\ (i\neq j, r_{ij}\leq2a) \tag{9b}$$

where $\mathbf{r}_{ij}$ is the distance between beads i and j, and $r_{ij}=|\mathbf{r}_{ij}|$. Brownian forces are coupled to these velocity perturbations through the fluctuation-dissipation theorem, and the distribution of $\mathbf{R}_i^n$ is Gaussian with zero mean and covariance, expressed as $\langle\mathbf{R}_i^n\mathbf{R}_j^n\rangle=2\mathbf{D}_{ij}^n\Delta t$.

In Eq. (7), the velocity fields $\mathbf{v}(\mathbf{r})=\mathbf{G}\cdot\mathbf{r}$ are given as $v_x=\dot{\gamma}y$ and $v_y=v_z=0$ for steady shear flow, and $v_x=\dot{\varepsilon}x$, $v_y=-\dot{\varepsilon}y/2$, and $v_z=-\dot{\varepsilon}z/2$ for uniaxial extensional flow, where $\dot{\gamma}$ and $\dot{\varepsilon}$ are the shear rate and elongation rate, respectively. Thus, the velocity gradient tensor $\mathbf{G}$ has the form

$$\mathbf{G}=\begin{bmatrix}0&\dot{\gamma}&0\\0&0&0\\0&0&0\end{bmatrix};\quad\mathbf{G}=\begin{bmatrix}\dot{\varepsilon}&0&0\\0&-\dot{\varepsilon}/2&0\\0&0&-\dot{\varepsilon}/2\end{bmatrix} \tag{10}$$

in simple shear and extensional flow, respectively.

With the spring force $\mathbf{F}_i^S$ associated with spring i, the effective spring force on bead i is given as

$$\mathbf{F}_i^{FENE}=\begin{cases}\mathbf{F}_1^S & i=1\\ \mathbf{F}_i^S-\mathbf{F}_{i-1}^S & 1<i<N\\ \mathbf{F}_{N-1}^S & i=N\end{cases} \tag{11}$$

One can apply the suitable model, depending on the force law used for the springs. In this study, springs with the distance $r_{i,i+1}$ between neighboring beads i and i+1 are assured by the finitely extendable nonlinear elastic (FENE) potential of Warner [28]

$$E_{i,i+1}^{FENE}=-(k_Sl_{max}^2/2)\ln[1-(r_{i,i+1}-l_0)^2/l_{max}^2] \tag{12}$$

where l_0 is the equilibrium bond length and l_{max} is the maximum bond length allowed. E^{FENE} is reduced to a harmonic potential with force constant k_S, in the limit of large l_{max}.

The Lennard-Jones (LJ) potential describing the dispersion-repulsion interaction between pairs of beads is taken by considering the energy parameter ε_{LJ} and the length scale σ_{LJ} set equal to $1.0k_BT$ and $1.0l_0$, respectively. The electrostatic interaction between beads is described via the screening Coulombic interaction, usually known as the Debye-Hückel (DH) potential:

$$E_{ij}^{ES}=\frac{q_b^2}{4\pi\varepsilon}\frac{e^{-\kappa r_{ij}}}{r_{ij}}=k_BTz_b^2\frac{l_B}{r_{ij}}e^{-\kappa r_{ij}}. \tag{13}$$

Here, q_b means the bead charge, the medium dielectric constant ε ($=\varepsilon_r\varepsilon_0$) is defined in terms of relative permittivity ε_r (=78.5 for water) and vacuum permittivity ε_0 ($=8.854\times10^{-12}$ C^2/J·m), and $z_b=q_b/e$ is the bead charge in units of elementary charge e ($=1.6\times10^{-19}$ C). $\kappa^{-1}=1/\sqrt{8\pi l_BN_AI}$ is the Debye screening thickness determined by Avogadro's number N_A, medium ionic strength I, and the Bjerrum length $l_B=e^2/4\pi\varepsilon k_BT$ (cf., $l_B=0.71$ nm at room temperature). In Fig. 2, the finite rigidity of the chain is modeled by the following harmonic bending potential:

$$E_{i,i+1}^{Bend}=(k_A\theta_{i,i+1}^2)/2 \tag{14}$$

where k_A is the bending force constant, $\theta_{i,i+1}=\cos^{-1}(\hat{b}_i\cdot\hat{b}_{i+1})$ is the angle between the two bond vectors, and the i-th bond vector of unit size is $\hat{b}_i=(\mathbf{r}_{i+1}-\mathbf{r}_i)/|\mathbf{r}_{i+1}-\mathbf{r}_i|$. The semiflexible and flexible chains are represented by each model with and without the bending potential between neighboring bonds, respectively.

2. Model Parameters

Information for dimension of xanthan chain was based on the approach of Chun and Park [29] as the average molecular weight of 1.13×10^6 g/mol (ca. 1220 monomers) with $l_P\cong120$ nm and $R_G\cong580$ nm at ionic strength I=100 mM. Considering the level of R_G/l_P, xanthan is modeled as a mesoscopic discrete chain with 25 beads ($N_b=25$), where about 10 beads represent a Kuhn segment length

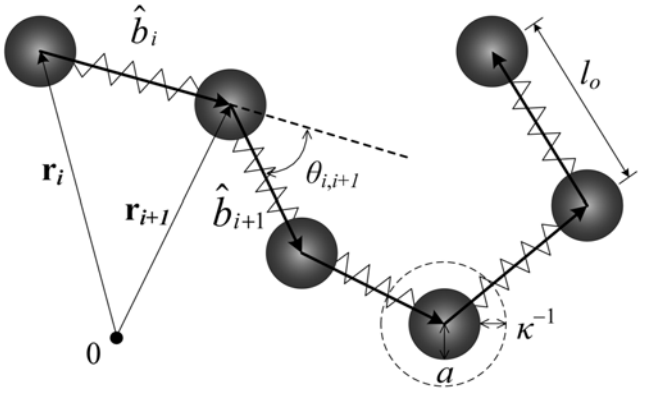

Fig. 2. Schematic of the bond vector and angle between beads.

($=2l_P$) ensuring a smooth persistence length variation according to environmental conditions. The bead hydrodynamic radius a chosen as 4 nm is determined by equating the volume of a circular cylinder with experimentally evaluated chain diameter d [30] and 580 nm length to the volume ($=(4\pi/3)(a^3N_b)$) of 25 beads. It is remarkable that the extension of xanthan at low I and a corresponding increase in the solution viscosity are likely to involve a transition of secondary structure (i.e., backbone conformation) from double strand to a disordered form with lower strandedness [31]. This denatured xanthan can undergo a disorder→order (i.e., coil→helix) transition when sufficient salt ion is present.

Conducting the previously described scheme [19], spring parameters (k_S, l_0, l_{max}, k_A) and z_b are optimized with preliminary BD simulations such that the chain reproduces experimental values of R_C and l_P at different screening thickness. We take the optimum stretching constant $k_S=2.5k_BT/l_0^2$, l_0=10 nm, and l_{max}=150 nm for semiflexible chain (cf., $k_S=3k_BT/l_0^2$, l_0=18 nm, l_{max}=40 nm for flexible chain). Note that the weak spring constant employed here is not so much a signature of entropic spring as a convenient way to take into account the nature of xanthan contour length. The optimal bead charge q_b of −35e for semiflexible chain corresponds to ~35% of the maximum value of −98e for the bead composed of 49 (=1,220/25) monomers, which leads to the contour distance per elementary charge l_q ($=R_C/(N_bz_b)$) of 0.66 nm. According to the Manning condensation [32], the minimum possible value of l_q in the presence of monovalent counterions is the Bjerrum length l_B (i.e., the length at which the screening energy equals to the thermodynamic energy). Therefore, it does not need to consider counterions since the parameterized bead charges include the possibility of counterion condensation. The optimized angle bending force constant determined as $k_A=4k_BT$ yields l_P=4b for a wormlike chain [14,33], which is close to the simulation result.

Under a given condition, 20 independent BD trajectories are analyzed for each of more than 10 msec in length. Integration time step Δt is chosen to satisfy the criterion $m_0/(6\pi\eta a)<<\Delta t<<6\pi\eta a^3/k_BT$ for the bead mass m_0. The simulation system is infinite in x and y directions. It is equilibrated for 2 msec (1×10^6 time steps) and the averages are taken for the next 14 msec (7×10^6 time steps).

RESULTS

1. Scaling Behavior of Conformation Properties

Scaling relations are first evaluated for the end-to-end distance, where a least squares fit gives the slope ($=2\nu$). Fig. 3 presents $\langle R_E^2\rangle$ versus N for various screening effects on a log-log plot. The exponents ν result in the range of 0.74-1.04 implying that ν is certainly higher than that of the flexible neutral chains in good solvent (i.e., ν=3/5). This should be one distinguishing characteristic of polyelectrolytes in solvent with infinite dilute concentration. The screening is almost complete at I=100 mM, in which this limit almost corresponds to the neutral scaling fit data. Debye thickness κ^{-1} (nm) is given by $[I(M)]^{-1/2}/3.278$ for ionic concentration of the symmetric monovalent electrolyte (or medium ionic strength). The I dependence on ν is evident, in which the ν value becomes higher as the screening effect (i.e., κ) decreases. This trend indicates that the degree of chain extensibility is becoming higher with decreasing screening effect.

In Fig. 4, the ν value for the radius of gyration is determined as

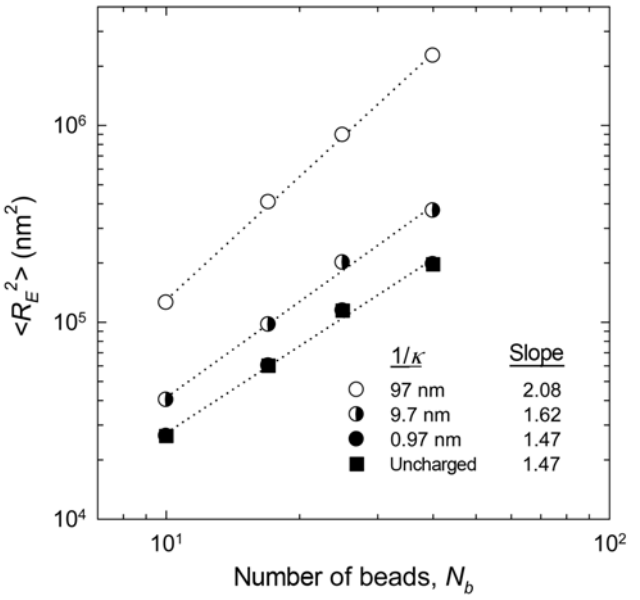

Fig. 3. The end-to-end distance versus the number of beads for different values of Debye screening thickness. κ^{-1} of 97, 9.7, and 0.97 nm corresponds to solution ionic concentration of 0.01, 1.0, 100 mM.

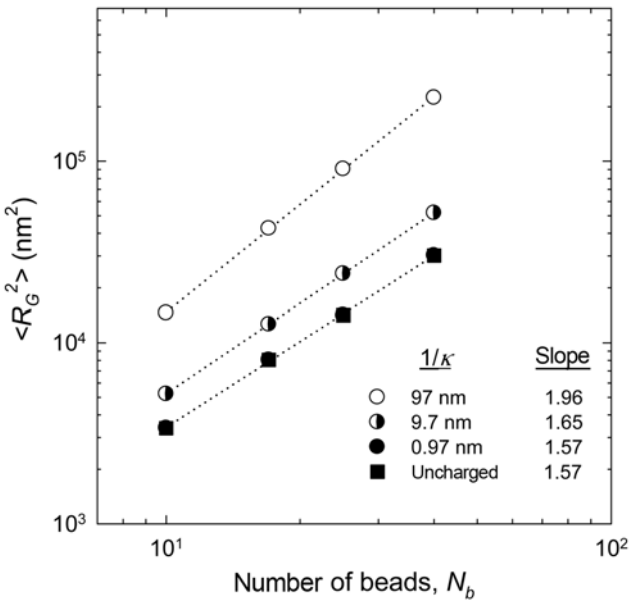

Fig. 4. The radius of gyration versus the number of beads for different values of Debye screening thickness κ^{-1} with the same condition of Fig. 3.

ranging 0.79-0.98, which can be a similar behavior to the case of end-to-end distance. The 3D extent of the chains can be examined by analyzing the moments of inertia. The average eigenvalues of the R_G^2 tensor scale as $R_x^2\sim R_y^2\sim R_z^2\sim N_b^{2\nu}$ with ν=1/2 and 3/5 for random walk of Gaussian (poor solvent) and SAW (good solvent) neutral chains, respectively. The scaling behavior of our results agrees with the literature data [3], where the longest axis grows like $R_x^2\sim N_b^2$ in the dilute limit. With increasing κ^{-1}, each semiflexible chain extends and $(R_E/R_G)^2$ could ideally converge to the value 12 for fully

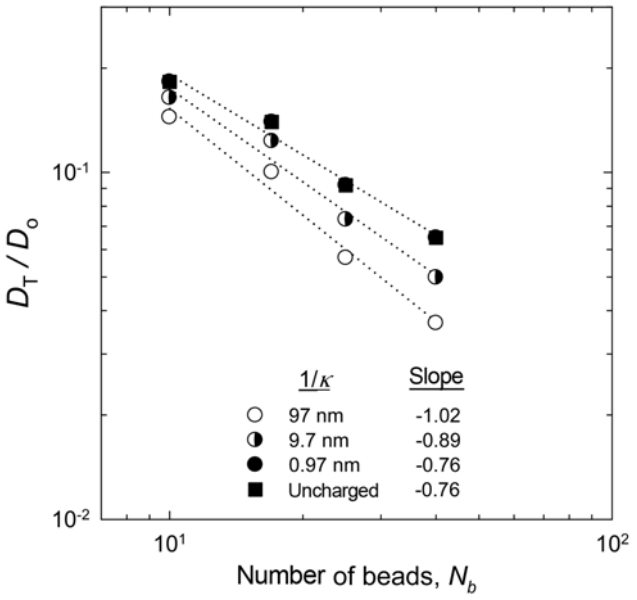

Fig. 5. The translational diffusion coefficient versus the number of beads for different values of Debye screening thickness κ^{-1} with the same condition of Fig. 3.

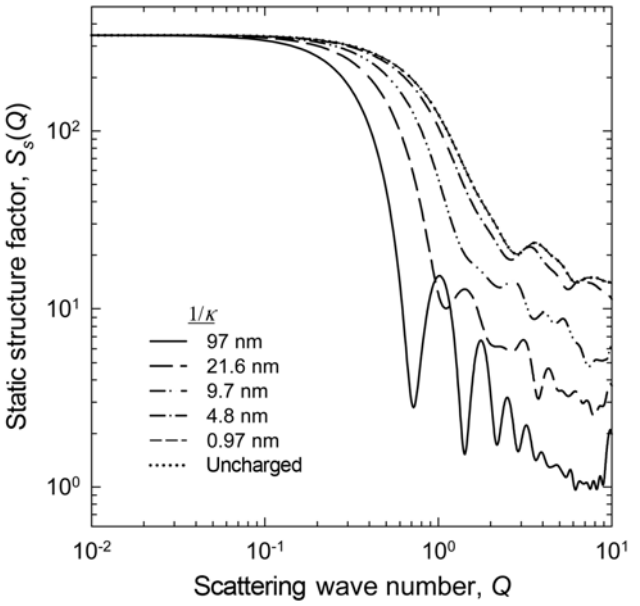

Fig. 6. Static structure factor $S_s(Q)$ of the N_b=25 chains for different values of Debye screening thickness κ^{-1} corresponding to I=0.01, 0.2, 1.0, 4.0, and 100 mM.

extended one.

In Fig. 5, the self-diffusion increases with decreasing κ^{-1} since the chain becomes more compact, where the diffusion of a single bead is estimated from $D_0=k_BT/6\pi\eta a$. The logarithmic slope of the diffusion data is −0.76 for neutral chain and −1.02 for charged chain of lower screening case (I=0.01 mM). Note that, for the case of the polymer chain without any excluded volume, Zimm obtained the preaveraged version of diffusion tensor, as given

$$\mathbf{D}_{ij}=\frac{1}{6\pi\eta}\left\langle\frac{1}{|\mathbf{r}_i-\mathbf{r}_j|}\right\rangle \quad i\neq j. \tag{15}$$

The diffusion coefficient of the chain is

$$D=\frac{D_0}{N_b}+\frac{k_BT}{6\pi\eta}\left\langle\frac{1}{r_H}\right\rangle \tag{16}$$

where r_H is the corrected hydrodynamic radius related to $\langle r_H^{-1}\rangle=N_b^{-2}\sum_{i,j}\langle r_{ij}^{-1}\rangle$. Since $\langle r_H^{-1}\rangle^{-2}$ is proportional to the mean square end-to-end distance $\langle R_E^2\rangle$ or the mean square radius of gyration $\langle R_G^2\rangle$ of the chain, one expects $D\propto N_b^{-\nu}$. Here, ν is again the universal exponent for the correlation length. Hence, scaling of diffusivity with N_b in this study deviates from existing theories, and the I dependence on ν shows the same trend observed in the case of chain conformation.

2. Structure Factor

To examine the chain conformation in detail at all length scales, the static structure factor of a single chain has been computed in our BD simulations. It is advantageous to consider the structure factor that makes theoretical prediction comparable to scattering experiments and is often an essential input into theoretical computations. The spherically averaged structure factor is defined with the wave vector **Q** in a reciprocal space, as

$$S_s(\mathbf{Q})\equiv\left\langle\frac{1}{N_b}\left|\sum_{l<m}^{N_b}\exp[i\mathbf{Q}\cdot(\mathbf{r}_l-\mathbf{r}_m)]\right|^2\right\rangle. \tag{17}$$

From the standpoint of more effective computations, $S_s(\mathbf{Q})$ can also be written as the following two-bead average:

$$S_s(\mathbf{Q})\equiv 1+\frac{1}{N_b}\sum_{l<m}^{N_b}\cos[\mathbf{Q}\cdot(\mathbf{r}_l-\mathbf{r}_m)]$$
$$=1+\rho\int_0^\infty[g(\mathbf{r})-1]\exp(i\mathbf{Q}\cdot\mathbf{r})d\mathbf{r} \tag{18}$$

where $g(\mathbf{r})$ is the pair correlation function [23,24].

Fig. 6 obtained from Eq. (18) shows oscillations, which are generally found in the dilute limit of polymer density. In the region of wave number Q more than about 0.1, $S_s(Q)$ clearly depends on the screening effect, showing that its value decreases with decreasing screening effect. The logarithmic slope between Q and $S_s(Q)$ data gives $-1/\nu$, which is again related to the chain conformations in terms of collapsed, totally stretched, and intermediate states. Considering the spherically averaged structure factor is almost usual, on which it is a well-known fact that a lower magnitude of the slope (i.e., higher ν) corresponds to a polyelectrolyte chain expanding with the SAWs conformation in good solvent condition. As the slope increases, a chain experiences the random walks in theta solvent condition that is a balanced state between the attraction and the repulsion, and ultimately the poor solvent condition with collapsed globular conformation is obtained.

However, it is difficult to observe clearly this behavior in a plot of Fig. 6, where the static structure factor parallel to the first principle axis of gyration is computed according to Eq. (18). Oscillations become pronounced with decreasing screening effect, as expected in a rigid rod chain. Increasing screening effect results in a shifting as well as a smearing out of these oscillations, which is consistent with the data reported in the literature [24].

CONCLUSIONS

The conformation and dynamics of single and semiflexible chains

of polyelectrolyte xanthan were simulated by applying a coarse-grained model with nonlinear bead-spring discretization of a whole chain. One of the important properties of polyelectrolytes is that they dissolve in water due to the interaction between monomers resulting in charged macroion and mobile counterions, even though water is a poor solvent for most of synthetic polymers. This study presents several key features of polyelectrolyte chains in solvent. From the scaling of R_E and R_G with respect to N_b, the Flory-Edwards exponent ν was found to be higher than that of the flexible neutral chains with SAW in good solvent, and its value increased with decreasing screening effect, representing the degree of chain extensibility.

Scaling behavior of translational diffusivity with N_b does not agree with existing theories for excluded-volume chains, i.e., Zimm prediction $D \propto N_b^{-\nu}$. In the structure factor parallel to the first principal axis of gyration, no clear scaling behavior with a well defined exponent shows up. While oscillations become pronounced with decreasing screening effect, they are tending toward a shifting and a smearing out with increasing screening effect. With viewing this present investigation as a first step, we will pursue and extend to more rigorous scaling behavior of polyelectrolyte in the future.

ACKNOWLEDGMENTS

This work was supported by the Nanotechnology Research Fund (No. 2008-02344) from the National Research Foundation of Korea.

REFERENCES

1. K. Kremer and K. Binder, *Comput. Phys. Rep*., **7**, 259 (1988).
2. D. A. Hoagland and M. Muthukumar, *Macromolecules*, **25**, 6696 (1992).
3. C. Holm, P. Këkicheff and R. Podgornik, Eds., *Electrostatic effects in soft matter and biophysics*, Vol. 46, NATO Science Series II: Mathematics, Physics and Chemistry, Kluwer, Dordrecht (2001).
4. A. V. Dobrynin and M. Rubinstein, *Prog. Polym. Sci*., **30**, 1049 (2005).
5. M. Daoud and P.-G. de Gennes, *J. Phys. France*, **38**, 85 (1977).
6. M. Doi and S. F. Edwards, *The theory of polymer dynamics*, Clarendon, Oxford (1986).
7. B. Li, N. Madras and A. D. Sokal, *J. Stat. Phys*., **80**, 661 (1995).
8. D. E. Smith, T. T. Perkins and S. Chu, *Macromolecules*, **29**, 1372 (1996).
9. P. J. Flory, *Principles of polymer chemistry*, Cornell Univ. Press, NY (1953).
10. T. Odijk, *J. Polym. Sci.: Polym. Phys. Ed*., **15**, 477 (1977).
11. J. H. van Vliet and G. ten Brinke, *J. Chem. Phys*., **93**, 1436 (1990).
12. A. Balducci, P. Mao, J. Han and P. S. Doyle, *Macromolecules*, **39**, 6273 (2006).
13. H. C. Öttinger, *Stochastic processes in polymeric fluids: Tools and examples for developing simulation algorithms*, Springer, Heidelberg (1996).
14. H. A. Jian, V. Vologodskii and T. Schlick, *J. Comput. Phys*., **136**, 168 (1997).
15. J. S. Hur, E. S. G. Shaqfeh and R. G. Larson, *J. Rheol*., **44**, 713 (2000).
16. R. M. Jendrejack, D. C. Schwartz, M. D. Graham and J. J. de Pablo, *J. Chem. Phys*., **119**, 1165 (2003).
17. R. M. D. Jendrejack, D. C. Schwartz, J. J. de Pablo and M. D. Graham, *J. Chem. Phys*., **120**, 2513 (2004).
18. Y. L. Chen, M. D. Graham, J. J. de Pablo, G. C. Randall, M. Gupta and P. S. Doyle, *Phys. Rev. E*, **70**, 060901R (2004).
19. J. Jeon and M.-S. Chun, *J. Chem. Phys*., **126**, 154904 (2007).
20. G. Paradossi and D. A. Brant, *Macromolecules*, **15**, 874 (1982).
21. T. Sato, T. Norisuye and H. Fujita, *Macromolecules*, **17**, 2696 (1984).
22. M.-S. Chun, C. Kim and D. E. Lee, *Phys. Rev. E*, **79**, 051919 (2009).
23. B. Dünweg and K. Kremer, *J. Chem. Phys*., **99**, 6983 (1993).
24. U. Micka and K. Kremer, *Phys. Rev. E*, **54**, 2653 (1996).
25. P.-K. Lin, C.-C. Fu, Y.-L. Chen, Y.-R. Chen, P.-K. Wei, C. H. Kuan and W. S. Fann, *Phys. Rev. E*, **76**, 011806 (2007).
26. D. L. Ermak and J. A. McCammon, *J. Chem. Phys*., **69**, 1352 (1978).
27. J. Rotne and S. Prager, *J. Chem. Phys*., **50**, 4831 (1969).
28. H. R. Warner, *Ind. Eng. Chem. Fund*., **11**, 379 (1972).
29. M.-S. Chun and O. O. Park, *Macromol. Chem. Phys*., **195**, 701 (1994).
30. B. T. Stokke, A. Elgsaeter, G. Skjåk-Brjek and O. Smidsrød, *Carbohydr. Res*., **160**, 13 (1987).
31. W. E. Rochefort and S. Middleman, *J. Rheol*., **31**, 337 (1987).
32. G. S. Manning, *J. Chem. Phys*., **51**, 924 (1969).
33. A. Dhar and D. Chaudhuri, *Phys. Rev. Lett*., **89**, 065502 (2002).